Physics Letters B 772 (2017) 290–293

Contents lists available at ScienceDirect

Physics Letters B

www.elsevier.com/locate/physletb

Chemical freeze-out in relativistic heavy-ion collisions

Jun Xu [a,*], Che Ming Ko [b]

[a] Shanghai Institute of Applied Physics, Chinese Academy of Sciences, Shanghai 201800, China
[b] Cyclotron Institute and Department of Physics and Astronomy, Texas A&M University, College Station, TX 77843, USA

ARTICLE INFO

Article history:
Received 19 April 2017
Received in revised form 31 May 2017
Accepted 21 June 2017
Available online 26 June 2017
Editor: W. Haxton

ABSTRACT

One surprising result in relativistic heavy-ion collisions is that the abundance of various particles measured in experiments is consistent with the picture that they reach chemical equilibrium at a temperature much higher than the temperature they freeze out kinetically. Using a multiphase transport model to study particle production in these collisions, we find, as an example, that the effective pion to nucleon ratio, which includes those from resonance decays, indeed changes very little during the evolution of the hadronic matter from the chemical to the kinetic freeze-out, and it is also accompanied by an almost constant specific entropy. We further use a hadron resonance gas model to illustrate the results from the transport model study.

The statistical model, which assumes that the abundance of particles produced in relativistic heavy-ion collisions or their chemical freeze-out is determined before the hadronic matter freezes out kinetically, has been very successful in describing the yields of particles measured in experiments. For heavy-ion collisions at the top energy of the Relativistic Heavy Ion Collision (RHIC) and the Large Hadron Collider (LHC) [1–3], the chemical freeze-out temperature extracted from the experimental data using the statistical model is around $160 \sim 170$ MeV and is similar to the critical temperature of the hadron–quark phase transition from lattice QCD calculations [1–4]. Although it is not known if the chemical freeze-out temperature in the collision energy regime of the RHIC Beam-Energy Scan (BES) program, which is around $140 \sim 160$ MeV, coincides with the hadron–quark phase boundary, relativistic heavy-ion collisions provide the only possibility to map out experimentally the phase diagram of the strong-interacting matter in the temperature (T) – chemical potential (μ) plane [5]. Since the chemical freeze-out temperature is much higher than that for the kinetic freeze-out, which is around $100 \sim 120$ MeV from the blast-wave model fit to experimental transverse momentum/mass spectra [6,7] and slightly decreases with increasing collision energy, to maintain the same relative abundance among various particles requires non-unity values for their fugacities as the hadronic matter expands and cools from the chemical freeze-out temperature $T_{\rm ch}$ to the kinetic freeze-out temperature $T_{\rm kin}$.

To study the origin of early chemical freeze-out, we use a multiphase transport model (AMPT) [8], which has been widely used as a theoretical tool or an event generator for relativistic heavy-ion collisions. In this model, the initial-state information is generated by the Heavy-Ion Jet INteraction Generator (HIJING) model [9], which is an extension of the PYTHIA model [10] for proton–proton collisions to nucleus–nucleus collisions. In the string melting version of AMPT, which is employed in the present study, all the hadrons produced from HIJING are converted into their valence quarks, and the dynamics of these quarks is described by Zhang's Parton Cascade (ZPC) model [11]. The parton scattering cross section is set to be 1.5 mb, which has been shown to reproduce reasonably well the experimentally measured collective flow in relativistic heavy-ion collisions [12]. The freeze-out of partons is determined by their last scatterings. Hadrons are then formed from a spatial coalescence model that converts two nearest quark and antiquark to a meson and three nearest quarks (antiquarks) to a baryon (antibaryon). The species of formed hadron is determined by the quark flavors and the invariant mass of these quarks. To reproduce reasonably the empirical energy density and/or temperature near hadronization, we remove the hadron formation time of 0.7 fm/c that is originally introduced in AMPT. The evolution of the hadronic phase is described by a relativistic transport (ART) model [13] that includes various hadron species and their elastic and inelastic scatterings as well as decays. The empirical energy dependence of the scattering cross sections, the Breit–Wigner mass distribution of resonances, and the mass dependence of the decay width are properly taken into account by satisfying the detailed balance condition, as described in Refs. [8,13]. The frequent scat-

* Corresponding author.
E-mail addresses: xujun@sinap.ac.cn (J. Xu), ko@comp.tamu.edu (C.M. Ko).

http://dx.doi.org/10.1016/j.physletb.2017.06.061

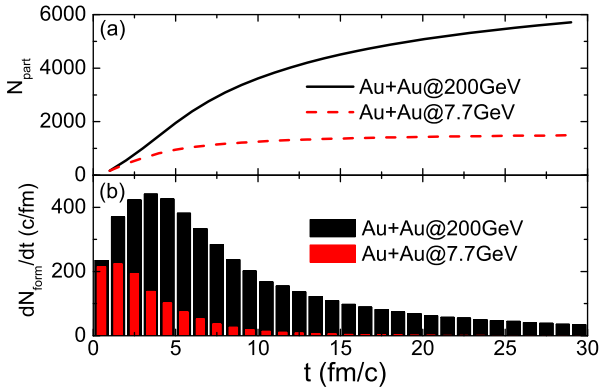

Fig. 1. (Color online). Time evolution of the total number of particles (a) and their formation rate (b) in the hadronic phase of central Au+Au collisions at $\sqrt{s_{NN}} = 200$ and 7.7 GeV.

terings among hadrons are helpful to maintain the thermal equilibrium in the hadronic phase. The AMPT model describes reasonably well measured rapidity distributions and transverse momentum spectra of pions, kaons, and protons in relativistic heavy ion collisions from RHIC-BES energies to top RHIC energy (see, e.g., Figs. (16–20) and Figs. (24–27) in Ref. [8]). Recently, the spatial coalescence model has been improved by relaxing the constraint of fixed numbers of mesons, baryons, and antibaryons [14], and it now gives an even better description of the relative particle ratios. In the present work we study central Au+Au collisions at center-of-mass energy $\sqrt{s_{NN}} = 200$ and 7.7 GeV, corresponding to the top RHIC energy and a typical lower collision energy at the RHIC-BES program where the partonic phase is less dominant. A total number of 100 and 1000 events are generated at $\sqrt{s_{NN}} = 200$ GeV and 7.7 GeV, respectively.

To give a general picture of particle production in the hadronic phase, we show in Fig. 1 the time evolution of the total number of particles and their formation rate in central Au+Au collisions from the AMPT model. It is seen that the total number of hadrons increases with time due to the continuous production of hadrons from quark coalescence as well as inelastic and decay channels in the hadronic phase. The different production times of hadrons from quark coalescence are a result of different quark freeze-out times from their last scatterings. Although the final hadron number is much larger at 200 GeV than at 7.7 GeV, hadrons are mostly formed at earlier times at lower collision energies due to the shorter lifetime of the partonic phase.

In Fig. 2, we show by filled squares the time evolution of the effective pion/nucleon ratio for collisions at both 200 GeV (left panel) and 7.7 GeV (right panel). In calculating the effective pion/nucleon ratio, we take into account those from the strong decays of resonances. Specifically, the pion-like particles include pions, Δ and N^* resonances, ρ mesons, ω mesons, η mesons, K^* mesons, and their antiparticles, while the nucleon-like particles include nucleons and their resonances Δ and N^*. Since the effective pion/nucleon ratio at kinetic freeze-out, when all resonances have already decayed, is the same as the real pion/nucleon ratio measured in experiments, a possible scenario in the transport model to justify the assumption of the statistical model that chemical freeze-out occurs before kinetic freeze-out is the constancy of the effective pion/nucleon ratio during hadronic evolution.

Since entropy is a thermodynamical quantity that contains information on both the number of degrees of freedom in a system and its degree of thermal equilibration, it is of interest to study this quantity in the hadronic phase of AMPT. Like the viscous effect in hydrodynamic description of heavy-ion collisions [15–18], entropy is produced in AMPT from scattering and production of particles.

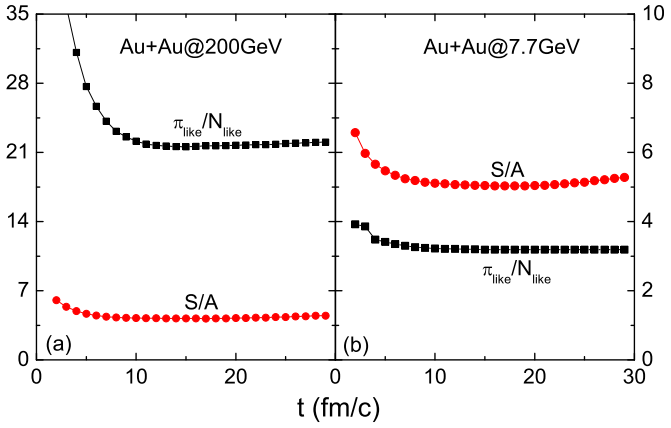

Fig. 2. (Color online). Time evolution of the specific entropy (S/A) and the effective pion/nucleon ratio (π_{like}/N_{like}) in the hadronic phase of central Au+Au collisions at $\sqrt{s_{NN}} = 200$ (a) and 7.7 GeV (b).

However, more entropy is expected to be produced in hadronic matter than in partonic matter because of its significantly larger specific viscosity [19]. Based on the thermal model, it has been shown that the specific entropy, i.e., the entropy per particle, is related to the deuteron/proton ratio in intermediate-energy heavy-ion collisions [20,21]. Therefore, the specific entropy and relative abundance of particle species in heavy-ion collisions are believed to be related, with the latter often used to extract the information about the former [22,23]. However, the relation between the specific entropy and the relative abundance of particles has so far been studied under the assumption that the system is in chemical equilibrium.

In the AMPT, the entropy can be calculated using the phase–space distributions $f_i(\mathbf{x}, \mathbf{p})$ of particle species i as in Refs. [24,25], i.e.,

$$S = -\sum_i g_i \int \frac{d^3\mathbf{x}d^3\mathbf{p}}{(2\pi)^3}[f_i \ln f_i \pm (1 \mp f_i)\ln(1 \mp f_i)], \qquad (1)$$

with g_i being the spin degeneracy of a hadron. For f_i in the above equation, it is evaluated from counting the number of particles in a local six-dimensional phase–space cell. The size of the phase–space cell is carefully chosen to be small but include sufficient number of particles after averaging over all events [25]. We use spherical coordinates for both position and momentum and divide the phase space into cells. Because of the symmetry in the azimuthal angle for central collisions, the dimension in the phase–space coordinate is reduced. We further introduce a momentum cut of $|p| < 4$ GeV/c in obtaining the results in Fig. 2 since low-momentum particles dominate at midrapidity. The entropy calculated from Eq. (1) is divided by the real particle number A contributing to the phase–space distribution f_i in order to get the specific entropy S/A. It is seen from Fig. 2 that the specific entropy and the effective pion/nucleon ratio decrease at the early stage of the hadronic phase, and both become approximately constant at later stage. The initial large specific entropy is due to the small number of particles and the dilute phase space, and this is also observed in Refs. [24,25]. It is also seen in Ref. [24] that both the pion/nucleon ratio and the specific entropy remain constant after the most compressed stage in intermediate-energy heavy-ion collisions, similar to the behavior in Fig. 2. Although this result seems to be consistent with the argument that the specific entropy is related to the relative abundance of particle species at and after chemical freeze-out [20–23], we will show later that the constant specific entropy and the constant effective pion/nucleon ratio cannot be achieved simultaneously unless the system becomes out

of chemical equilibrium in later stage. However, we can still define the chemical freeze-out time, which is about 8 fm/c at $\sqrt{s_{NN}} = 200$ GeV and about 6 fm/c at 7.7 GeV, indicated in Fig. 3 by filled squares and circles, respectively, after which the effective pion/nucleon ratio remains essentially unchanged. It is also seen that it takes a longer time to reach chemical freeze-out at 200 GeV than at 7.7 GeV, and this is due to the earlier production of hadrons at lower collision energies as shown in Fig. 1.

Results from AMPT, which does not assume thermal and chemical equilibrium, can be qualitatively understood in terms of the hadron resonance gas model that includes all the hadron species in the ART/AMPT model. For such a system containing non-interacting hadrons, the number density ρ, the energy density ϵ, and the entropy density s can be respectively expressed as [26,27]

$$\rho = \sum_i g_i \int \frac{d^3p}{(2\pi)^3} f_i, \tag{2}$$

$$\epsilon = \sum_i g_i \int \frac{d^3p}{(2\pi)^3} f_i \sqrt{m_i^2 + p^2}, \tag{3}$$

$$s = -\sum_i g_i \int \frac{d^3p}{(2\pi)^3} [f_i \ln f_i \pm (1 \mp f_i)\ln(1 \mp f_i)], \tag{4}$$

with m_i being the mass of hadron species i. The occupation number of hadrons in momentum is given by

$$f_i = \frac{1}{\lambda_i \exp[(\sqrt{m_i^2 + p^2} - \mu_i)/T] \pm 1}, \tag{5}$$

where $\mu_i = B_i\mu_B + C_i\mu_c$ is the chemical potential of particle species i, with B_i and C_i being its respective baryon and charge numbers, μ_B and μ_c being its respective baryon and charge chemical potentials, and λ_i is the fugacity that takes into account the possible violation of chemical equilibrium. In the above equations, the upper signs are for fermions and the lower signs are for bosons. The charge chemical potential μ_c is determined by the charge conservation condition $\rho_c/\rho_B = 79/197$ for Au+Au collisions, with the charge density ρ_c and the net baryon density ρ_B calculated similarly as Eq. (2). The specific entropy S/A from the hadron resonance gas model is s/ρ. Including the same pion-like and nucleon-like particles as in the AMPT calculations and assuming that they are in separate chemical equilibrium, their fugacities can be written as $\lambda_i = \lambda_N^{z_N}\lambda_\pi^{z_\pi}$, where z_N (z_π) is the effective nucleon (pion) number. For instance, we have $z_N = 1$ and $z_\pi = 1$ for Δ resonances, and $z_N = 0$ and $z_\pi = 2$ for ρ mesons.

We first evaluate the energy density ϵ and the net baryon density ρ_B in the central sphere of radius $r = 5$ fm in the hadronic phase of AMPT, and the results are shown in the upper panel of Fig. 3. We then use the hadron resonance gas model to obtain from ϵ and ρ_B the temperature, and its time evolution is shown in the lower panel of Fig. 3. For collisions at both $\sqrt{s_{NN}} = 200$ and 7.7 MeV, the highest energy density of about 0.65 GeV/fm^3 is seen to correspond to the highest temperature of about 152 MeV. The chemical freeze-out temperature T_{ch} is 141 MeV at 200 GeV at about $t = 8$ fm and 134 MeV at 7.7 GeV at about $t = 6$ fm, which are slightly lower than those extracted from the experimental data based on the statistical model [1,2,6,28,29].

Using an initial state that is in chemical equilibrium with its thermodynamical properties given by filled symbols in Fig. 3, we then study the evolution of the system in its specific entropy, effective pion/nucleon ratio, volume, and fugacities of pion-like and nucleon-like particles as it cools down in a hadron resonance gas model for three different scenarios. In the first scenario of keeping the constant effective pion/nucleon ratio by adjusting the volume

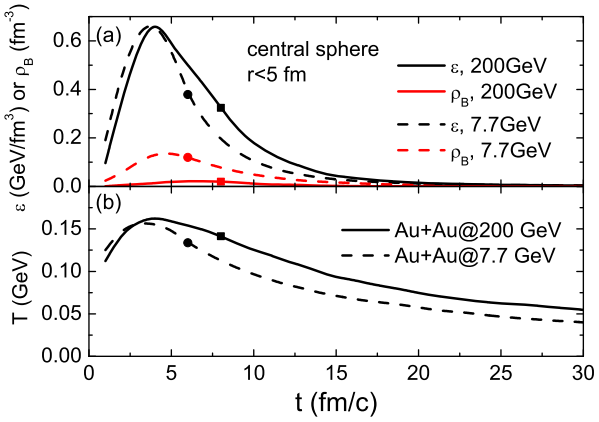

Fig. 3. (Color online). Time evolution of the energy density ϵ and the net baryon density ρ_B (a) in the central sphere of radius $r = 5$ fm in the hadronic phase of central Au+Au collisions at $\sqrt{s_{NN}} = 200$ and 7.7 GeV as well as the extracted temperature (b) from the hadron resonance gas model. Filled squares and circles indicate the time after which the effective pion/nucleon ratio and the specific entropy remain approximately constant.

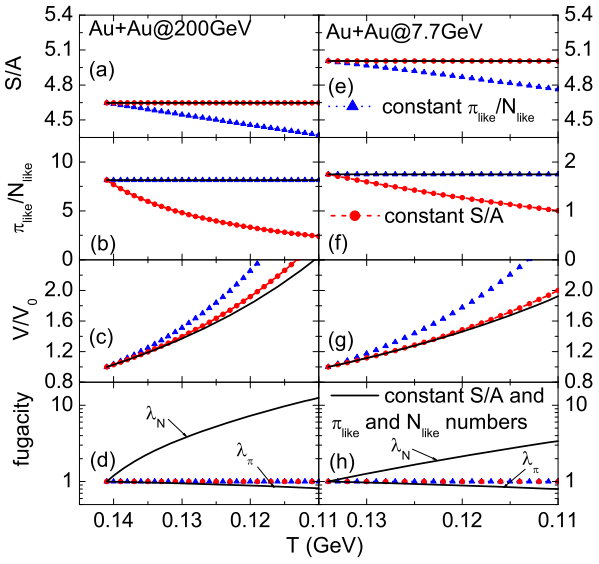

Fig. 4. (Color online). Evolution of the specific entropy (first row), the effective pion/nucleon ratio (second row), the volume (third row), and the fugacities for pion-like and nucleon-like particles (bottom row) as the hadron resonance gas cools with its volume and/or the values of particle fugacities varied to keep a constant effective pion/nucleon ratio (filled triangles), a constant specific entropy (filled circles), or the constancy of both (solid lines). See text for details.

V of the hadronic matter relative to its initial volume V_0 at chemical freeze-out, shown by filled triangles in Fig. 4, the specific entropy decreases as the system cools down. In the second scenario of keeping the specific entropy a constant with a smaller change in volume, shown by filled circles in Fig. 4, the effective pion/nucleon ratio decreases. To keep both the specific entropy and the effective pion/nucleon ratio constant as in Fig. 2 from the AMPT model, it is necessary to introduce non-unity values for the fugacity parameters. Here we assume that all pion-like and nucleon-like particles are not in chemical equilibrium while their effective numbers remain the same after initial chemical freeze-out, although in more general case both would increase but with their ratio remaining a constant. It is seen from the solid lines in Fig. 4 that in this third scenario the system becomes increasingly out of chemical equilibrium during its expansion and cooling as indicated by increasing nucleon and decreasing pion fugacities away from unity.

To summarize, we have investigated the chemical freeze-out conditions in relativistic heavy-ion collisions based on a multiphase transport model. Despite the continuous production of hadrons, the chemical freeze-out time can be determined when the effective pion/nucleon ratio becomes a constant. The latter is also found to be accompanied by a constant specific entropy. Starting from the chemical freeze-out state in the AMPT model, we have further studied the expansion and cooling of the system using the hadron resonance gas model, and found that only the scenario of an expanding and cooling hadronic matter with non-unity fugacities can lead to both constant specific entropy and effective pion/nucleon ratio. Our study shows that after chemical freeze-out in relativistic heavy-ion collisions, the system is no longer in chemical equilibrium, but the statistical model can still be used to extract the temperature and chemical potential at chemical freeze-out since the relative abundances of particle species remain constant during later hadronic evolution. The present study thus helps clarify our understanding of chemical freeze-out in relativistic heavy-ion collisions, and validate the use of the statistical model in mapping out the phase diagram of the strong-interacting matter from relativistic heavy-ion collisions.

We thank Chen Zhong for maintaining the high-quality performance of the computer facility. The work of JX was supported by the Major State Basic Research Development Program (973 Program) of China under Contract Nos. 2015CB856904 and 2014CB845401, the National Natural Science Foundation of China under Grant Nos. 11475243 and 11421505, the “100-talent plan” of Shanghai Institute of Applied Physics under Grant Nos. Y290061011 and Y526011011 from the Chinese Academy of Sciences, the Shanghai Key Laboratory of Particle Physics and Cosmology under Grant No. 15DZ2272100, and the “Shanghai Pujiang Program” under Grant No. 13PJ1410600, while that of CMK was supported by the US Department of Energy under Contract No. DE-SC0015266 and the Welch Foundation under Grant No. A-1358.

References

[1] J. Adams, et al., STAR Collaboration, Nucl. Phys. A 757 (2005) 102.
[2] K. Adcox, et al., PHENIX Collaboration, Nucl. Phys. A 757 (2005) 184.
[3] B. Abelev, et al., ALICE Collaboration, Phys. Rev. C 88 (2013) 044910.
[4] F. Karsch, Lect. Notes Phys. 583 (2002) 209.
[5] Y. Akiba, et al., arXiv:1502.02730 [nucl-th].
[6] L. Adamczyk, et al., arXiv:1701.07065 [nucl-ep].
[7] L. Kumer, Nucl. Phys. A 931 (2014) 1114.
[8] Z.W. Lin, C.M. Ko, B.A. Li, B. Zhang, S. Pal, Phys. Rev. C 72 (2005) 064901.
[9] X.N. Wang, M. Gyulassy, Phys. Rev. D 44 (1991) 3501.
[10] http://home.thep.lu.se/~torbjorn/Pythia.html.
[11] B. Zhang, Comput. Phys. Commun. 109 (1998) 193.
[12] J. Xu, C.M. Ko, Phys. Rev. C 84 (2011) 014903.
[13] B.A. Li, C.M. Ko, Phys. Rev. C 52 (1995) 2037.
[14] Y.C. He, Z.W. Lin, arXiv:1703.02673 [nucl-th].
[15] A. Hosoya, K. Kajantie, Nucl. Phys. B 250 (1985) 666.
[16] P. Danielewicz, M. Gyulassy, Phys. Rev. D 31 (1985) 53.
[17] H. Heiselberg, X.N. Wang, Phys. Rev. C 53 (1996) 1892.
[18] A. Muronga, Phys. Rev. Lett. 88 (2002) 062302;
A. Muronga, Phys. Rev. Lett. 89 (2002) 159901 (Erratum);
A. Muronga, Phys. Rev. C 69 (2004) 034903.
[19] N. Demir, S.A. Bass, Phys. Rev. Lett. 102 (2009) 172302.
[20] P.J. Siemens, J.I. Kapusta, Phys. Rev. Lett. 43 (1979) 1486.
[21] J. Aichelin, E.A. Remler, Phys. Rev. C 35 (1987) 1291.
[22] K.G.R. Doss, et al., Phys. Rev. C 37 (1988) 163.
[23] C. Kuhn, et al., Phys. Rev. C 48 (1993) 1232.
[24] K.K. Gudima, et al., Phys. Rev. C 32 (1985) 1605.
[25] G. Bertsch, J. Gugnon, Phys. Rev. C 24 (1981) 2514.
[26] P. Braun-Munzinger, K. Redlich, J. Stachel, in: R. Hwa, X.N. Wang (Eds.), Quark Gluon Plasma 3, World Scientific, Singapore, 2004, p. 491, arXiv:nucl-th/0304013.
[27] A. Andronic, P. Braun-Munzinger, J. Stachel, Nucl. Phys. A 772 (2006) 167.
[28] J. Cleymans, H. Oeschler, K. Redlich, S. Wheaton, Phys. Rev. C 73 (2006) 034905.
[29] A. Andronic, P. Braun-Munzinger, J. Stachel, Nucl. Phys. A 834 (2010) 237c.